JVSTB Journal of Vacuum Science & Technology B

Optical transitions in magnetoelectric Ga0.6Fe1.4O3 from 0.73 to 6.45 eV

Sukgeun Choi, Christophe Lefèvre, Francois Roulland, Christian Mény, Nathalie Viart, Bobby To, Devyn E. Shafer, Ranhee Shin, Jihye Lee, and William Jo

Citation: Journal of Vacuum Science & Technology B **30**, 041204 (2012); doi: 10.1116/1.4721649

View online: http://dx.doi.org/10.1116/1.4721649

View Table of Contents: http://scitation.aip.org/content/avs/journal/jvstb/30/4?ver=pdfcov

Published by the AVS: Science & Technology of Materials, Interfaces, and Processing

Optical transitions in magnetoelectric $Ga_{0.6}Fe_{1.4}O_3$ from 0.73 to 6.45 eV

Sukgeun Choi
National Renewable Energy Laboratory, Golden, Colorado 80401

Christophe Lefèvre, Francois Roulland, Christian Mény, and Nathalie Viart
Institute of Physics and Chemistry of Materials of Strasbourg, UMR 7504 ULP-CNRS, 23 rue du Loess, B.P. 43, 67034, Strasbourg Cedex 2, France

Bobby To and Devyn E. Shafer
National Renewable Energy Laboratory, Golden, Colorado 80401

Ranhee Shin, Jihye Lee,[a] and William Jo[b]
Department of Physics, Ewha Womans University, Seoul 120-750, South Korea

(Received 20 March 2012; accepted 9 May 2012; published 25 May 2012)

The optical properties of polycrystalline $Ga_{0.6}Fe_{1.4}O_3$ bulk are determined by spectroscopic ellipsometry from 0.73 to 6.45 eV. Complex dielectric function $\varepsilon = \varepsilon_1 + i\varepsilon_2$ spectra are obtained from the multilayer analysis. The ellipsometric data exhibit numerous optical structures, and the transition energies are accurately obtained by analyzing the second-energy derivatives of the data. The origins of the optical structures are explained in terms of Fe^{3+} ligand field transitions and ligand-to-metal charge transfer transitions. © *2012 American Vacuum Society*.
[http://dx.doi.org/10.1116/1.4721649]

I. INTRODUCTION

There is a growing interest in the electrical manipulation of magnetic states through magnetoelectric coupling for potential applications in next generation memory devices.[1] To realize this new kind of functional device with the desired level of performance, however, the discovery of materials exhibiting strong magnetoelectricity above room temperature is a prerequisite. For this purpose, the transition metal oxide $Ga_{2-x}Fe_xO_3$ receives considerable attention.[2–7] The oxide $Ga_{2-x}Fe_xO_3$ $(0.8 \leq x \leq 1.4)$ possesses ferrimagnetic and pyroelectric characteristics with a strong coupling between the magnetic and electric properties at high temperature.[3]

Another potential application of $Ga_{2-x}Fe_xO_3$ is in photovoltaic devices as is $BiFeO_3$.[8–10] For materials with no inversion center of symmetry, photogenerated electrons and holes can be separated spontaneously by the polarization (P_s) presented in the crystal without need of a *p–n* junction.[9] The larger P_s leads to the better charge separation, and the calculated P_s value for $BiFeO_3$ single crystal[11] is 90–100 $\mu C/cm^2$ along the principal axis (the [111] axis in the *pseudocubic* rhombohedral structure). Results from a recent local spin density approximation (LSDA + U) of density functional theory predict that the P_s in $GaFeO_3$ is 58.63 $\mu C/cm^2$ in the [010] axis.[12]

In understanding the electronic structure and related physical properties of materials, spectroscopic information plays an important role. For example, pronounced optical structures in dielectric function $\varepsilon = \varepsilon_1 + i\varepsilon_2$ spectra generally stem from band-to-band transitions in semiconductors and charge transfer transitions in transition-metal complexes. As a result, experimentally determined ε spectra are widely used to verify the predictions made by electronic structure calculations of materials.[13]

Spectroscopic ellipsometry (SE) determines accurately the ε spectra of materials over a wide photon energy range, and it has been used for optical studies of numerous material systems.[14] Even though iron-oxide and related compounds such as $BiFeO_3$ (Refs. 15–17) have been investigated systematically by SE, studies of $Ga_{2-x}Fe_xO_3$ are rare. Kalashnikova *et al.*[5] reported SE-determined anisotropic ε spectra of orthorhombic $GaFeO_3$ and trigonal $Ga_{0.25}Fe_{1.75}O_3$ single crystals from 0.7 to 5.4 eV. However, their *pseudodielectric function* $\langle\varepsilon\rangle = \langle\varepsilon_1\rangle + i\langle\varepsilon_2\rangle$ spectra show nonzero $\langle\varepsilon_2\rangle$ values below the absorption edge, which perhaps stem from surface-overlayer artifacts such as microscopic roughness, native oxides, or any kind of surface perturbation. In addition, no rigorous spectral analysis was attempted in their work, and thus our knowledge of optical transitions in $Ga_{2-x}Fe_xO_3$ is still very limited.

Here, we present the optical information of $Ga_{0.6}Fe_{1.4}O_3$ obtained by analyzing the SE data. This particular chemical composition $x = 1.4$ is of great interest for device applications since its Curie temperature was measured to be 370 K, and the room-temperature saturated magnetization was as high as 90 emu/cm^3 in the thin film phase.[7] However, $Ga_{0.6}Fe_{1.4}O_3$ has not been examined by SE yet.

Our study has a twofold primary goal—to determine reference quality optical function spectra and to accurately obtain optical transition energies. We model the SE-determined $\langle\varepsilon\rangle$ spectra using multilayer analysis with the B-spline formulation.[18] The spectra exhibit several optical structures, and their energy values are obtained by the standard line shape analysis.[19] The possible origins of the observed optical transitions are attributed to the Fe^{3+} ligand field (*d–d*) transitions in the low-energy (<3 eV) region and to ligand-to-metal charge transfer (LMCT) transitions in the high-energy (>3 eV) region.[20]

[a]Present address: Max Planck Institute of Microstructure Physics, D-06120 Halle, Germany.
[b]Author to whom correspondence should be addressed; electronic mail: wmjo@ewha.ac.kr

II. EXPERIMENT

A disk-shape ($\varnothing = 15$ mm and $d = 2$ mm) polycrystalline $Ga_{0.6}Fe_{1.4}O_3$ bulk was prepared by using a sintering process. The stoichiometric milling of Fe_2O_3 and Ga_2O_3 was carried out in an attritor mill for 1 h in an ammoniacal solution (pH = 9). The solution was then kept inside a drying oven until the liquid part was completely evaporated. The resulting powder was manually ground and an organic binder (polyvinyl alcohol) of around 3 wt. % was added to improve the mechanical properties of the sample. The powder was finally compacted into pellets and sintered in a platinum crucible for 40 h at 1400 °C and then for another 10 h at 1450 °C, both in air.

Formation of a single phase of $Ga_{0.6}Fe_{1.4}O_3$ with orthorhombic structure was verified explicitly by x-ray diffraction (XRD) θ–2θ scans using a Bruker D8 Advance equipped with a monochromatic Cu radiation source ($K\alpha = 1.54056$ Å) and a Sol-X detector. The 2θ scan range was from 25° to 40° and the angular resolution was 0.02°. Profile matching refinement was performed by the FULLPROF program[21] using the pseudo-Voigt profile function. The XRD pattern in Fig. 1 shows the peaks characteristic of the $GaFeO_3$ structure (space group $Pna2_1$) and there is no evidence of the presence of impurities. The refinement of the XRD data results in the lattice parameters $a = 8.762(1)$Å, $b = 9.419(1)$Å, and $c = 5.083(1)$Å.

SE data were acquired from 0.73 to 6.45 eV using a spectroscopic rotating compensator-type ellipsometer (M2000-DI model, J.A. Woollam Inc.) with the sample at room temperature. The angle of incidence was varied from 65° to 75° with an increment of 5°. Data were recorded after averaging 5000 cycles of the compensator (5000 revolutions per measurement) to increase the signal-to-noise ratio.

III. RESULTS AND DISCUSSION

The ε spectra of $Ga_{0.6}Fe_{1.4}O_3$ are extracted by multilayer (ambient/surface–roughness/bulk) analysis of the SE data. The microscopic roughness of the surface, estimated to be ~50 Å, is represented by a Bruggeman effective medium approximation using a 50–50 mixture of the bulk and void.[22] The optical functions of the $Ga_{0.6}Fe_{1.4}O_3$ bulk are constructed by the B-spline formulation.[18] The SE data Ψ and Δ taken at three incident angles and their best-fit curves are shown as open symbols and closed lines, respectively, in Figs. 2(a) and 2(b). Only 10% of the actual data points are presented here to show clearly the quality of the fits.

Figure 2(c) presents the resulting ε spectra. As mentioned earlier in this paper, the $Ga_{2-x}Fe_xO_3$ ($0.8 \le x \le 1.4$) bulk crystallizes in the orthorhombic structure and thus biaxial optical anisotropy ($\varepsilon_{xx} \neq \varepsilon_{yy} \neq \varepsilon_{zz}$) is anticipated in theory. The polycrystalline nature of the $Ga_{0.6}Fe_{1.4}O_3$ used in our study, however, makes it difficult to probe the optical anisotropy. Therefore, our ε spectra reported here can be regarded as an average of the three principal components, $(\varepsilon_{xx} + \varepsilon_{yy} + \varepsilon_{zz})/3$. We note that the SE study of Kalashnikova *et al.*[5] has found no strong anisotropy in orthorhombic $GaFeO_3$ crystal. Thus, $Ga_{0.6}Fe_{1.4}O_3$ crystal studied in this work, which also forms in the orthorhombic structure, may not exhibit strong optical anisotropy either.

In Fig. 2(c), two major optical structures are seen at ~3.5 and 6.0 eV with a distinct but relatively weak shoulder at ~2.4 eV. The inset shows two additional weak features, E_a

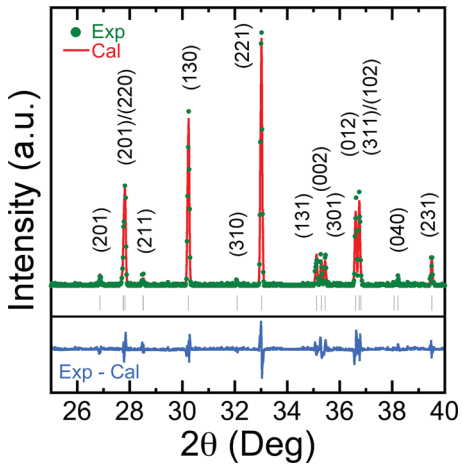

FIG. 1. (Color online) X-ray diffraction pattern of $Ga_{0.6}Fe_{1.4}O_3$ bulk. Experimental data (solid green circles) are in an excellent agreement with the calculated curve (solid red line). Vertical thin lines below the experimental data indicate the Bragg reflections, and the solid blue curve (Exp - Cal) in the bottom part.

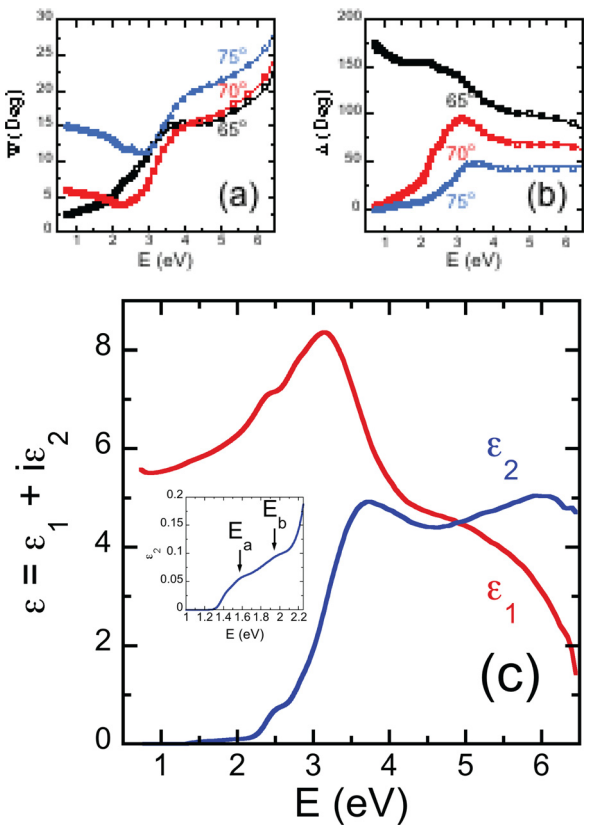

FIG. 2. (Color online) Data (open symbols) and the best-fit curves (solid lines) for (a) Ψ and (b) Δ of $Ga_{0.6}Fe_{1.4}O_3$. Only 10% of the data points are presented to show clearly the quality of fit. (c) Dielectric function $\varepsilon = \varepsilon_1 + i\varepsilon_2$ spectra obtained from the multilayer analysis. Inset: The ε_2 spectrum from 1.0 to 2.2 eV shows two weak structures, E_a and E_b, at ~1.55 and ~1.95 eV, respectively.

and E_b, at ~1.55 and ~1.95 eV in the ε_2 spectrum, respectively. The two major structures in the high-energy (>3 eV) region are attributed to the superposition of multiple LMCT transitions from the O 2*p* bands to the Fe 3*d* bands.[20] They rather appear as broad structures in the room-temperature ε spectra, but the individual transitions are better resolved in the derivative spectra, which is discussed later.

The three weak structures in the low-energy (<3 eV) region were identified as the Fe^{3+} ligand field transitions.[5,20,23,25,26] In the octahedral field (O_h symmetry), the five *d* orbitals—d_{xy}, d_{yz}, d_{zx}, $d_{x^2}-d_{y^2}$, and d_{z^2}—are split into two sets of levels, t_{2g} (d_{xy}, d_{yz}, and d_{zx}) and e_g ($d_{x^2}-d_{y^2}$ and d_{z^2}), as depicted in Fig. 3(a). The ground state $^6A_1$ arises from the $(t_{2g})^3(e_g)^2$ configuration of high-spin Fe^{3+}, where three unpaired electrons occupy the three t_{2g} levels and the remaining two unpaired electrons the two e_g levels. The first possible excited state configuration is $(t_{2g})^4(e_g)$,[1] which results in the $^4T_1$ and $^4T_2$ states. The next excited state is predicted to be the $^4A_1$,^4E states with the $(t_{2g})^3(e_g)^2$ configuration. Conclusively, the first three optical transitions observed at ~1.55, ~1.95, and ~2.4 eV are attributed to the $^6A_1 \rightarrow {}^4T_1$,$^6A_1 \rightarrow {}^4T_2$, and $^6A_1 \rightarrow {}^4A_1$,$^4E$ transitions, respectively.[5,23,25,26] The ligand field transitions from the ground state to excited states and the electronic configurations[24] of each state are depicted in Fig. 3(b).

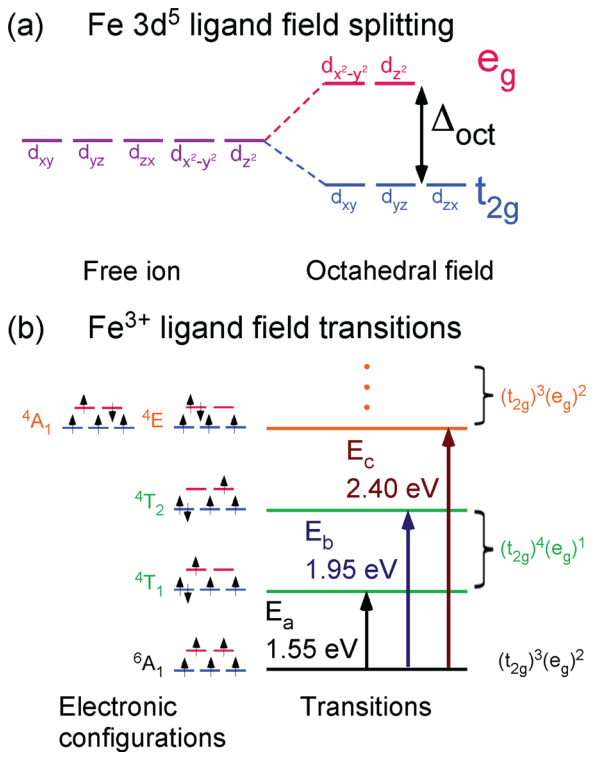

FIG. 3. (Color online) (a) Fe $3d^5$ ligand field splitting. The degenerated five 3*d* orbitals are split into two levels, t_{2g} and e_g, in the octahedral field. The energy difference between those two levels is the octahedral field splitting parameter Δ_{oct}. (b) Simplified Tanabe–Sugano diagram (Ref. 23) for Fe^{3+} in the octahedral coordination. The three weak transitions at ~1.55, ~1.95, and ~2.4 eV observed in the ε_2 spectrum [in Fig. 2(c)] are identified as the $^6A_1 \rightarrow {}^4T_1$,$^6A_1 \rightarrow {}^4T_2$, and $^6A_1 \rightarrow {}^4A_1$,$^4E$ transitions, respectively. The electronic configurations of each state are also included (Ref. 24).

These ligand field transitions from the ground state $^6A_1$ to the excited states are, in principle, forbidden by the selection rules.[20] First, all the transitions within the *d*-shell are not allowed because the quantum number must be changed ($\Delta l = \pm 1$). Second, the spin selection rule ($\Delta S = 0$) states that there should be no change in the number of unpaired electrons (multiplicity). However, these forbidden ligand field transitions are often observed in iron oxides through the magnetic coupling of electronic spins of next nearest neighbor Fe^{3+} cations in the crystal structure,[23] although their intensities are much weaker than the allowed LMCT transitions as revealed in Fig. 2(c).

In order to accurately determine energies of the optical structures in the high-energy region (LMCT transitions), we numerically calculated second-energy-derivative spectra from the $\langle\varepsilon\rangle$ data using a linear filtering algorithm of the Savitzky–Golay type.[27] The LMCT transition energies are then extracted by least-squares fitting the standard line shape expressions to the data.[17,19] Both real and imaginary parts were fitted simultaneously. The second-energy-derivative spectra of the $\langle\varepsilon\rangle$, together with the best-fit curves, are shown in Fig. 4. The open circles and squares represent the $d_2\langle\varepsilon_1\rangle/dE^2$ and $d_2\langle\varepsilon_2\rangle/dE^2$ results, respectively, which are calculated from the data. The solid-red and dotted-blue lines correspond to the best-fit curves of the real and imaginary parts, respectively.

Differentiation enhances the sensitivity to the residual optical structures, and multiple LMCT transitions are now clearly shown in Fig. 4. For example, a weak spectral feature locating at 2.72 eV is not seen in the ε spectra in Fig. 2(c), but its existence (E_d transition) is obvious in the $d_2\langle\varepsilon\rangle/dE^2$ spectra. This structure has not been resolved in the previous SE study[5] of $GaFeO_3$. A total of seven line shapes are employed to fit the spectra between 2.0 and 6.0 eV. The fit-determined energies of these transitions are listed in Table I. For comparison, the energies for $GaFeO_3$ and $Ga_{0.25}Fe_{1.75}O_3$ reported in previous studies[5,25,26] are also included.

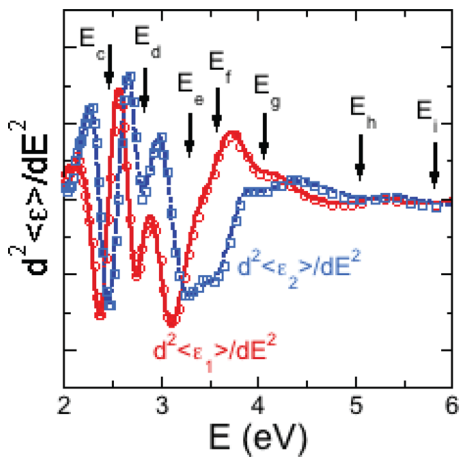

FIG. 4. (Color online) Solid and dotted lines are standard line shapes fit to second-energy-derivative $d_2\langle\varepsilon_1\rangle/dE^2$ (open circles) and $d_2\langle\varepsilon_2\rangle/dE^2$ (open squares) spectra, respectively. For clarity, only one-third of the actual data points are shown. The energies of each transition are indicated by arrows. Note: The labels are given in an arbitrary manner; they are irrelevant to the group theory representations.

TABLE I. Optical transition energies for $Ga_{0.6}Fe_{1.4}O_3$ at room temperature (in eV). Previously reported energies for $GaFeO_3$ and $Ga_{0.25}Fe_{1.75}O_3$ are also included for comparison.[a]

		$Ga_{0.4}Fe_{1.6}O_3$	$GaFeO_3$			$Ga_{0.25}Fe_{1.75}O_3$
	Transitions	This work	Reference 26	Reference 25	Reference 5[b]	Reference 5[b]
Ligand field transitions	E_a $^6A_1 \rightarrow {}^4T_1$	~1.55	1.5	1.55	~1.5	
	E_b $^6A_1 \rightarrow {}^4T_2$	~1.95	2.18	1.95	~2.0	
	E_c $^6A_1 \rightarrow {}^4A_1, {}^4E$	2.40 ± 0.01		2.84	~2.5	2.53 (*xx*) 2.53 (*zz*)
Charge transfer transitions	E_d $t_{2u}(\pi) \rightarrow t_{2g}$	2.72 ± 0.01				2.84 (*xx*) 2.99 (*zz*)
	E_d $t_{1u}(\pi) \rightarrow t_{2g}$	3.10 ± 0.02			3.3 (*xx*) 3.28 (*yy*) 3.31 (*zz*)	3.16 (*xx*) 3.32 (*zz*)
	E_f $t_{1u}(\sigma) \rightarrow t_{2g}$	3.70 ± 0.04			3.6 (*xx*) 3.9 (*yy*) 3.69 (*zz*)	3.86 (*xx*) 3.88 (*zz*)
	E_g $t_{2u}(\pi) \rightarrow e_g$	4.13 ± 0.04				4.63 (*xx*)
	E_h $t_{1u}(\pi) \rightarrow e_g$	4.96 ± 0.29				4.63 (*zz*)
	E_i $t_{1u}(\sigma) \rightarrow e_g$	5.85 ± 0.01			5.4 (*xx*) 6.0 (*yy*) 6.0 (*zz*)	5.9 (*xx*) 5.92 (*zz*)

[a]Suggested origins of each transition are given based on the results from electronic structure calculations (Refs. 5 and 28).
[b]The parentheses given with the energy values from Ref. 5 indicate the components of anisotropic ε data.

The first transition E_c at 2.4 eV in Fig. 4 is the Fe^{3+} ligand field transition $^6A_1 \rightarrow {}^4A_1, {}^4E$, which has already been explained in Fig. 3(b). The E_d transition occurring at 2.72 eV is the LMCT transition with the smallest energy in $Ga_{0.6}Fe_{1.4}O_3$, and therefore this is somewhat equivalent to the fundamental bandgap in band-to-band transition materials. Our value is close to the optical gap energy reported by Sun *et al.*[26] on $GaFeO_3$ thin film deposited on quartz substrate, 2.76 eV, but much larger than the theoretical prediction[12] of ~2 eV. Observation of discrepancy between theoretical prediction and experimental determination of bandgap energy is not unusual, which can be understood by the underestimation of bandgap energies in many density functional theory calculations.[12]

For higher-energy (>3 eV) optical structures in $GaFeO_3$, a recent first-principles calculation[12] attributed those to the transitions from the uppermost valence band mainly consisting of Fe 3*d* and O 2*p* states to the conduction band with Fe 3*d*, Ga 4*s*, Ga 4*p*, and O 2*p* states. More detailed information on the optical transitions in trigonal-phase $Ga_{0.25}Fe_{1.75}O_3$ has been given by Kalashnikova *et al.*[5] based on the results from calculations of the electronic structure of iron oxide (α-Fe_2O_3) within the cubic-field approximation.[28]

However, orthorhombic-phase $Ga_{2-x}Fe_xO_3$ ($0.8 \leq x \leq 1.4$) compounds possess different crystallographic symmetries from trigonal-phase $Ga_{0.25}Fe_{1.75}O_3$, and their optical transitions in high-energy regime are not clearly understood yet. Positive identification of the origin of these transitions would require rigorous theoretical investigations, which is beyond the scope of this work. Rather, it is our intention to report accurate energy value of optical transitions in $Ga_{0.6}Fe_{1.4}O_3$, so that theoreticians can perform calculations and fine adjustments of the electronic structure of orthorhombic-phase $Ga_{2-x}Fe_xO_3$ compounds.

IV. CONCLUSIONS

We reported complex dielectric function ε spectra of the polycrystalline $Ga_{0.6}Fe_{1.4}O_3$ bulk from 0.73 to 6.45 eV. We applied the multilayer modeling procedures to extract the ε spectra from the ellipsometric data. The spectra exhibit several optical structures, and their energies were obtained from the standard line shape analysis of second-energy-derivative $d_2\langle\varepsilon\rangle/dE^2$ spectra. Three relatively weak structures at ~1.55, ~1.95, and 2.40 eV are identified as the Fe^{3+} ligand transitions. The next six structures at 2.72, 3.10, 3.70, 4.13, 4.96, and 5.85 eV are assigned to various ligand-to-metal charge transfer transitions from O 2*p* bands to Fe 3*d* bands. Our findings provide ample incentive to better understand the electronic structure and related physical properties of orthorhombic-phase $Ga_{2-x}Fe_xO_3$ as a research path to developing high-performance magnetoelectric and photovoltaic devices.

ACKNOWLEDGMENTS

This work was supported by the Leading Foreign Research Institute Recruitment Program through the National Research Foundation of Korea (NRF) funded by the Ministry of Education, Science and Technology (MEST)

(2011-00267). The work done at National Renewable Energy Laboratory (NREL) is supported by the U.S. Department of Energy under Contract No. DE-AC36-08GO28308.

[1]M. Bibes and A. Barthélémy, Nature Mater. **7**, 425 (2008).
[2]J. P. Remeika, J. Appl. Phys. **31**, 263S (1960).
[3]T. Arima *et al*., Phys. Rev. B **70**, 064426 (2004).
[4]J. H. Jung, M. Matsubara, T. Arima, J. P. He, Y. Kaneko, and Y. Tokura, Phys. Rev. Lett. **93**, 037403 (2004).
[5]A. M. Kalashinikova, R. V. Pisarev, L. N. Bezmaternykh, V. L. Temerov, A. Kirilyuk, and Th. Rasing, JETP **81**, 452 (2005).
[6]M. J. Han, T. Ozaki, and J. Yu, Phys. Rev. B **75**, 060404R (2007).
[7]M. Trassin *et al*., J. Mater. Chem. **19**, 8876 (2009).
[8]W. Ji, K. Yao, and Y. C. Liang, Adv. Mater. **22**, 1763 (2010).
[9]S. Y. Yang *et al*., Nat. Nanotechnol. **5**, 143 (2010).
[10]H. T. Yi, T. Choi, S. G. Choi, Y. S. Oh, and S.-W. Cheong, Adv. Mater. **23**, 3403 (2011).
[11]J. B. Neaton, C. Ederer, U. V. Waghmare, N. A. Spaldin, and K. M. Rabe, Phys. Rev. B **71**, 014113 (2005).
[12]A. Roy, S. Mukherjee, R. Gupta, S. Auluck, R. Prasad, and A. Garg, J. Phys.: Cond. Mat. **23**, 325902 (2011).
[13]See, for example, S. Adachi, *Optical Constants of Crystalline and Amorphous Semiconductors: Numerical Data and Graphical Information* (Kluwer, Boston, 1999).
[14]D. E. Aspnes, in *Handbook of Optical Constants of Solids*, edited by E. D. Palik (Academic, Orlando, 1985), Vol. I, Chap. 5.
[15]R. V. Pisarev, A. S. Moskvin, A. M. Kalashinikova, and Th. Rasing, Phys. Rev. B **79**, 235128 (2009).
[16]J. F. Ihlefeld *et al*., Appl. Phys. Lett. **92**, 142908 (2008).
[17]S. G. Choi, H. T. Yi, S.-W. Cheong, J. N. Hilfiker, R. France, and A. G. Norman, Phys. Rev. B **83**, 100101R (2011).
[18]B. Johs and J. S. Hale, Phys. Status Solidi A **205**, 715 (2008).
[19]M. Cardona, *Modulation Spectroscopy*, Solid State Physics Supplement 11, edited by F. Seitz, D. Turnbell, and H. Ehrenreich (Academic, New York, 1969).
[20]A. B. P. Lever, *Inorganic Electronic Spectroscopy*, 2nd ed. (Elsevier, Amsterdam, 1984).
[21]J. Rodríguez-Carvajal, Physica B **192**, 55 (1993).
[22]D. E. Aspnes, Thin Solid Films **89**, 249 (1982).
[23]D. M. Sherman, Phys. Chem. Miner. **12**, 161 (1985).
[24]R. G. Burns, *Mineralogical Applications of Crystal Field Theory*, 2nd ed. (Cambridge University Press, Cambridge, 1993), p. 58.
[25]Y. Ogawa, Y. Kaneko, J. P. He, X. Z. Yu, T. Arima, and Y. Tokura, Phys. Rev. Lett. **92**, 047401 (2004).
[26]Z. H. Sun, S. Dai, Y. L. Zhou, L. Z. Cao, and Z. H. Chen, Thin Solid Films **516**, 7433 (2008).
[27]A. Savitzky and M. J. E. Golay, Anal. Chem. **36**, 1627 (1964).
[28]A. I. Likhtenshtein, A. S. Moskvin, and V. A. Gubanov, Sov. Phys. Solid State **24**, 2049 (1982).